On the Design of Active Contours for Medical Image Segmentation

A Scheme for Classification and Construction

T. M. Lehmann, J. Bredno, K. Spitzer
Institute of Medical Informatics, Aachen University of Technology, Aachen, Germany

Summary

Objectives: To provide a comprehensive bottom-up categorization of model-based segmentation techniques that allows to select, implement, and apply well-suited active contour models for segmentation of medical images, where major challenges are the high variability in shape and appearance of objects, noise, artifacts, partial occlusions of objects, and the required reliability and correctness of results.

Methods: We consider the general purpose of segmentation, the dimension of images, the object representation within the model, image and contour influences, as well as the solution and the parameter selection of the model. Potentials and limits are characterized for all instances in each category providing essential information for the application of active contours to various purposes in medical image processing. Based on prolaps surgery planning, we exemplify the use of the scheme to successfully design robust 3D-segmentation.

Results: The construction scheme allows to design robust segmentation methods, which, in particular, should avoid any gaps of dimension. Such gaps result from different image domains and value ranges with respect to the applied model domain and the dimension of relevant subsets for image influences, respectively.

Conclusions: A general segmentation procedure with sufficient robustness for medical applications is still missing. It is shown that in almost every category, novel techniques are available to improve the initial snake model, which was introduced in 1987.

Keywords

Image processing, computer-assisted (tree number L01.700.568.110.308), algorithms (tree number L01.700.568.110.050), finite element analysis (tree number H01.548.350)

Methods Inf Med 2003; 42: 89–98

Introduction

Model-based segmentation methods are commonly used in medical imaging. In contrast to pixel-, edge-, texture-, or region-based methods, the model-based approach is capable of including a-priori knowledge that significantly increases robustness. Model-based segmentation consists of two parts. First, a more or less strict assumption is selected to describe relevant objects. This description uses an abstract representation of the object to be segmented and defines its data structure. Subsequently, model-based segmentation is the search for the specific instance of the model, which best explains the image values (1). Therefore, the second part of model-based segmentation is the algorithm used to determine this specific instance.

One early and well known method of model-based segmentation is the "snake" introduced in 1987 by Kass, Witkin and Terzopoulos (2). Snake-based segmentation optimizes a list of vertices so that these vertices are positioned at high local gradients in the image and that the contour's first- and second-order derivatives are small. The a-priori knowledge available for this model are coherence and smoothness of object's borders and occurrence of significant changes in image values at its borders.

Development of model-based segmentation has taken place for more than a decade (3). Many – it seems far too many – models have been presented in the literature. In particular, active contours are often applied to medical images because they are capable of successfully operating on this type of data (4). In medical imaging, objects of interest have a large variability of shape and appearance. Their contours are often disturbed by noise, partial occlusions, or other artifacts. Nevertheless, medical image processing must be reliable and reproducible to significantly support diagnosis or research. Hence, robust and efficient active contours for general purpose are still missing (5). Automated segmentation – as important as it may be – still lacks robust realization (6). The well established snake is the basis for new developments, e.g. (7) and remains the reference to evaluate models that are developed more than ten years later, e.g. (8).

Surveys on model-based segmentation usually are focused on certain fields of application, e.g. (9, 10, 11). Mostly, they present the field of research top-down, guided by some particular examples and hence, they show ambiguities among each other. A detailed bottom-up classification of methods, which is required for the design of medical applications, is not provided. However, two elemental groups of model-based techniques are recognized (12):

- *Active contour models* have a preferably high degree of freedom in order to represent any possibly desired object contained in an image.
- *Shape-based models* represent an a-priori defined class of objects with preferably few degrees of freedom.

An overview of shape-based models including the active shape pioneered by Cootes et al. (13) and other shape representations with few degrees of freedom like deformable Fourier models, e.g. (14) is given in (10).

Objectives

This paper is focused on the design of active contours for medical applications. Useful categories are provided for systematical classification of methods. In each of

Received January 16, 2002
Accepted June 24, 2002

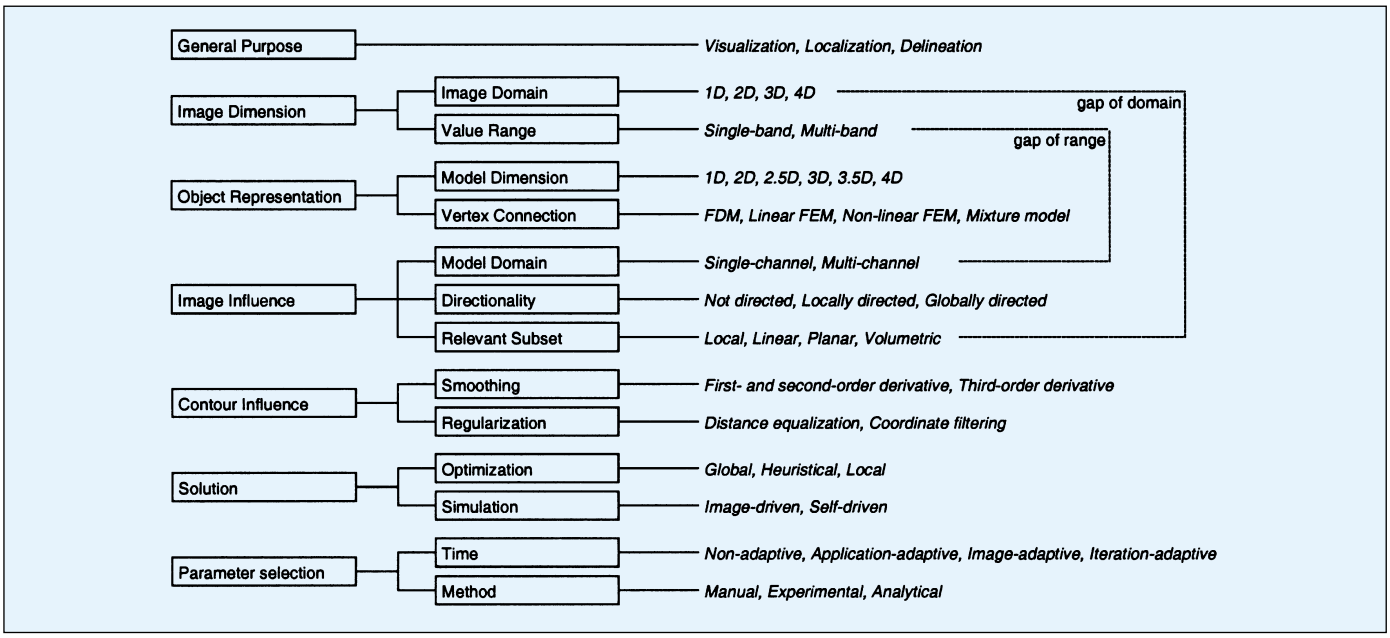

Fig. 1 Classification of active contour models. Abbreviations: xD – x-dimensional, FDM – finite difference model, FEM – finite element model

the unambiguous categories, general characteristic properties are derived and examples are given. This enables both user and developer to design the best suited method for a certain application. This goal is accomplished by characteristic references denoted ",e.g. (x)" although we do not aim to provide a complete survey of model-based segmentation.

Categorization of Active Contour Models

Figure 1 presents seven distinct categories, which describe the properties of model-based segmentation methods. Most of them are separated into sub-categories with unambiguous instances.

General Purpose of Segmentation

Segmentation is the basis of image analysis systems and the general purpose of the system mainly determines the superior model. However, the goal itself is often not taken into account when a model for segmentation is selected and implemented. Vermuri and Guo have identified three instances in this category (15).

In some applications, the selection of structures is required for their presentation to the user or physician. Here, coherent and smooth structures are of major interest (16). Depending on the method of *visualization*, this is possible without the determination of location and contour of objects. A segmentation prior to visualization allows to correct errors from pixel classification, which, for example, are inherent to volume-based visualization.

Usually, objects are described by their mean position and, if necessary, their size and orientation (17, 18). Such compact information is required for automated quantification and measurements but does not support a detailed description of shape. Although manual *localization* is quite simple, automatic localization is one of the most difficult tasks in medical image processing (19). Since localization strongly reduces information, models with few degrees of freedom are successfully applied. In other words, shape-based models are often superior to active contours for localization.

A *delineation* provides detailed geometric information on the contour of relevant structures. Hence, all image elements have to be assigned either to objects or to the background. In order to reproduce local details, many degrees of freedom are needed. Therefore, active contours are predominantly used for delineation. This requires a-priori localization, which might be provided manually by the user, e.g. (2, 20) or automatically by application-specific methods, e.g. (21). Note that contrarily to computer applications, it is most difficult for humans to provide reproducible delineation.

Image Dimension

Active contour segmentation strongly depends on the dimension of image material. The **image domain** is defined as the set of points for which measurements are provided by the imaging modality. Two-dimensional (2D) problems are still regarded as the major challenge in medical image processing (22). For sequences of planar images, which are usually acquired with different inter- and intra-slice resolution, tracking, e.g. (23, 24) or volumetric segmentation (25) is applied, while sequences of volumetric data assign time-variable image values to positions in four-dimensional (4D) space, e.g. (26 - 28).

The **value range** is the set of possible values that can be assigned to points in the image domain, e.g. scalar (*single-band*) or vectored (*multi-band*).

Object Representation

An active contour is represented by a list of positions of vertices in the image domain. Segmentation adapts these positions to the image data. Hence, the **model dimension** specifies the degree of freedom for each vertex, i.e., the number of independent directions, a vertex is allowed to move (Table 1). Note however that the dimension of the model does not necessarily equal the dimension of image domain. A one-dimensional (1D) application is the automated delineation after a manual initialization, where each vertex is moved on a straight line perpendicular to the initial contour (29) or the active-rays, i.e., a polar-transformed active contour (32). 2D-models, such as the original snake (2), are most frequently applied in medical image processing. The per-se coherence of segmentation (30) is lost when planar representations are applied to 3D-images (21). Propagation methods are often chosen to re-introduce spatial or temporal coherence, e.g., a slice-wise 2D-segmentation is used as initialization of the subsequent slice (31).

Different approaches are used to **connect** the active contour's **vertices**. Only a list of vertices is used by a finite difference model (*FDM*) (36). The FDM-vertices are also referred to as snaxels (snake elements) (37). Snaxels must have small distances (25) and their number is often fixed, e.g. (38).

An extension of FDMs for active contours has been introduced by Pentland et al. (39) and Cohen and Cohen (25): The finite element model (FEM) additionally includes edge elements with simulated material properties. The connecting edge elements (edgels) become the active part of the representation (33). FEMs approximate sections of the quasi-continuous contour using piecewise definitions (27). Often, a *linear FEM* is applied. In two dimensions, this yields polygonal models, e.g. (40, 41). For volumetric images, the resulting contour is a triangulated surface (28). Such explicit surfaces modeled by a list of similar elements (42) also exist as three-dimensional (3D) simplex-meshes where each vertex is connected to exactly three others (43). However, the term "simplex-mesh" is not used unambiguously in this context. All linear FEMs are $C^{(1)}$-discontinuous at vertices and between adjacent triangles. The discontinuities can be solved by *non-linear* approximations of finite elements, such as piecewise polynomials. In two dimensions, splines or similar interpolation functions are used to ensure $C^{(1)}$-continuity, e.g. (20, 44). In three dimensions, splines, e.g. (26) and quintic finite elements (45) are used to model active contours. Other edge instances of object representations are neither linear nor polynomial.

A *mixture model* is based on a combination of FDMs and FEMs. For instance, FEM-contours in one slice are FDM-connected to contours in adjacent slices (33), or vertices of a FEM-contour in three dimensions are FDM-connected to contours of prior or later points in time, e.g. (26). Gunn and Nixon use dual active contours describing two approaching FDM-contours on the inside and outside of objects connected by a FEM with linear connecting elements in between (4). Pixel-based contours are another possible intermediate in this category, e.g. (46, 47). A pixel-based contour is defined by adjacent vertex positions only and the vertices themselves are connecting elements.

Table 1
Exemplary active contour models of different model dimension

dimension	references
1D	(32, 29)
2D	(2, 30, 21)
2.5D (propagation)	(31, 18, 24, 33)
3D	(34, 35, 21)
3.5D (propagation)	(26, 27)
4D	(28)

Image Influences

One main part of all active contours is the interpretation of image values. We use the term image influence as a generalization for external energy, external force, image energy, image force and many others because none of these terms is used unambiguously in literature.

The **model domain** describes the ability of active contours to deal with multi-band images. *Single channel* models analyze scalar image values only. Even for the segmentation of multi-band images, single-channel models form the majority of active contours. Any multi-band information is transformed into a scalar prior to segmentation, e.g. (48, 49). For example, color information is disregarded if a single-channel model is used (50). Only a few *multi-channel* models read image information from independent image bands (51 - 53).

Furthermore, it is important to consider the **directionality** of image influences. Scalar (i.e. *not directed*) influences, such as an energy, discard any directional information of gradients (54). They provide a quality measure for vertices according to their current position in the image. By means of scalar edge filters, e.g. (2, 12, 30), which often are based on the first- or second-order derivative (33), it is determined whether each pixel or voxel belongs to an object's border. The absolute value of the edge filter is identified as an image potential or an external energy (51).

For *locally directed* image influences, the match between the local direction of the contour and the direction of edges in the image is taken into account. Directed image influences, such as forces, are defined by the scalar product of the contour's normal vector and the image's gradient, e.g. (31, 40). This results in an interpretation of image values adaptive to the direction of the contour (21, 34, 55).

Globally directed influences determine the direction of vertices towards relevant edges in the entire image. Binary pressure, also referred to as region-based force, forms the most frequently used variant (51, 52, 56, 57). Binary pressure discriminates image values from the inside and outside of objects. Image values belonging to the inside result in image influences pushing the contour outwards and vice versa. Alterna-

tively, globally directed influences are computed from a potential image that gives a gradient in direction of relevant edges for all points in the image, e.g. the distance transform of edge-filtered images, the gradient vector flow (54), or the optical flow to track image sequences (24).

To compute both directed and undirected image influences, image values have to be evaluated in the vicinity of vertices. The quality of detection significantly depends on the dimension of **relevant subsets** (58). *Local* (0D) image information is read only at the vertex' position. Although the model runs in danger of missing relevant image information, local influences are mostly used for active contours, e.g. (2, 24). This risk further increases (33) if model-based segmentation of 3D-images relies on local influences, e.g. (40, 45). Instead, image information can also be read from a *linear* (1D) subset, e.g. a line perpendicular to the contour. *Planar* (2D) image information is used when a small region around each vertex is evaluated. In image domains of higher dimension, even *volumetric* (3D & 4D) subsets are possible (Table 2).

Contour Influence

During the iterative movement, contour influences are needed to smooth the contour and to unify the discrete contour's representation. Again, the term contour influence is introduced as a generalization to avoid ambiguities found in literature for terms like internal energy, internal force, deformation energy and many others. Note that such influences do not necessarily result in an internal force or energy.

For **smoothing**, the contour itself is modified. In 1986, Terzopoulos presented a method for the reconstruction of continuous and discontinuous data points (63). For the snake model, these data points became high local gradients in the image and the contour influence became the internal energy written as a locally weighted sum of first- and second-order derivatives. Based on mechanics, the thin-plate model assigns material properties to a contour (9). The minimization of the *first- or second-order derivative* simulates the elasticity or rigidity of material, respectively. For 3D-models, vertices do not have well-defined predecessors and successors. Therefore, approximations are needed to compute the local second-order derivative. The star-shaped vicinity of vertices in triangulated surface can be used to compute contour influences (64). Angles and distances to all neighboring vertices are used in the resulting umbrella-operator (65). The minimization of the second-order derivatives applied to volumetric images or image sequences corresponds to the material rigidity or simulates the inertia of moved masses, respectively.

Lobregt and Viergever suggested a new formulation to smooth an active contour. The second-order derivative is not minimized but allowed to change moderately along the contour (66). Note that this is tantamount to the minimization of the contour's *third-order derivative*. It is accomplished by computing local forces that result from material rigidity and then using a high-pass filter for these forces such that local details are preserved without global smoothing. As another variant, local curvatures are trained from examples (61). The contour influence is then computed from distances to exemplary contours.

Depending on the formulation of image influences, vertices may aggregate in some sections of the contour (32). Subsequent computation of discrete derivatives then becomes numerically unstable (37). This instability can be controlled either by resampling during the iteration or by adding contour influences that direct vertices towards a uniform discretization of the contour. For such a **regularization**, influences are derived either from *distance equalization,* e.g. (31, 43) or from low-pass *filtering* of the vertices' *coordinates,* e.g. (34). In general, regularization causes only minor changes of the represented object even though vertex positions may strongly vary.

Table 2 Exemplary active contour models of different dimensions of the relevant image subset

image subset	dimension	Reference
local	0D	(2, 24, 40, 45)
linear	1D	(55, 59, 57, 36)
planar	2D	(51, 49, 60, 61)
volumetric	3D & 4D	(62, 28)

Solution to the Segmentation Task

Active contours require an algorithm to determine the instance that best explains the image values according to the a-priori knowledge of the model.

Optimization methods describe this quality of a contour by quantitative measures, such as energies (2). Then, segmentation corresponds to the optimization of the contour's energy.

Only for some special variants of active contours and by use of strict assumptions for the objects occurring in the image, a *global* extremum of a quality measure yields precise delineation of relevant objects. For global optimization, simulated annealing or stochastic relaxation techniques are used, e.g. (44, 47).

More frequently, the search space is not convex (67). Therefore, it is too complex for common optimization methods to find the global extremum (29). Since many local optima exist, segmentation is achieved by selecting a certain local extremum (44). *Heuristical* optimization methods are capable of skipping minor local optima. Numerical solution schemes include the combination of the Euler-Lagrange equation with some heuristic task-specific adaptations, as reviewed in the paper of McInerney and Terzopoulos, e.g. (7, 37, 68, 69) and dynamic programming[1], e.g. (8). However, heuristic optimization techniques need to increase their convergence radius (70). This radius

[1] Note that dynamic programming is often not the appropriate term for the myopic optimization schemes proposed in some of the given references, as dynamic programming in general is used to locate an absolute extremum.

gives the maximum distance between initialization and solution in search space so that a desired local optimum is found. Up to now, the convergence radius of active contours using optimization schemes is too small for reproducible automated segmentations (54).

All other optimization methods are only suitable to find the next *local* optimum within the convergence radius of the initialization. For an automated delineation, a localization has to be given by a user. Malladi, Sethian and Vemuri refer to this manual localization as initial guess (46). The segmentation strongly depends on this initial guess which must be close to the final solution (35). Although manual initialization can be done easily for planar images, it is rather cumbersome for volumetric or higher-dimensional data-sets (71).

Simulation methods use physically plausible model assumptions to describe a time-dependent behavior of active contours (72). In each iteration, directional influences are determined for all vertices. Vertices move until they are stopped by these influences at the border of objects. Such models are also known as geometrically deformed models or dynamic active contours (66).

Physically plausible model assumptions are often derived from mechanics but also from thermodynamics, e.g. (46). For mechanical models, vertices are moved by *image-driven* forces reaching an equilibrium for the final contour position (25). The forces result from the image data and simulated material properties. Movements can be computed either proportional to the sum of all forces, e.g. (25, 73) or by a simulated inert mass, e.g. (66). In the latter case, damping is needed to stop the contour at an object's border (40). The simulation itself can be performed individually for every vertex, e.g. (60) or using the explicit Euler scheme, e.g. (74). In both cases, the movement per step has to be small in order to obtain a stable behavior of the model (65).

One main advantage of simulation methods is the ability to formulate *self-driven* seeking tendencies that make the contour move when it is not in the vicinity of relevant image information. Mostly, pressure is used as seeking tendency (25) beside all other image-driven forces. Vertices can move for long distances until they contact relevant image information. Therefore, self-driven simulation methods allow changes in size and shape of active contours with high convergence radii.

Parameter Selection

Active contours incorporate competing influences resulting from the image, contour regularization, and seeking tendencies. The parameter selection assigns weights to all influences that are incorporated into the model. These weights have major impact on the quality of segmentation.

Parameters can be set at different **times** during the design or application of the model. During the development of a model, a strategic choice of parameters is based on either theoretical or experimental results and is fixed for all applications and images (*non-adaptive*). If parameters only show minor influences on the segmentation, they will never be changed. More frequently, the selection of parameters is performed once for every application of a model to instance a-priori knowledge on the certain application (7). *Image-adaptive* parameterization individually sets parameters for every image. This is required whenever *application-adaptive* segmentation fails due to the variety of image appearances in a certain application (75). Sometimes, parameters are changed during the segmentation itself. Such *iteration-adaptive* parameterization depends on the number of iterations, e.g. (69), the size of the contour, e.g. (76), or the image values that are read from the relevant subset, e.g. (51).

In addition, different **methods** are in use to set the parameters of an active contour model regardless of the point of time the parameterization is performed. For instance, parameters are manually changed until the segmentation complies with the visual impression of the user.

Manual parameterization, also referred to as ad-hoc (59) or trial-and-error parameterization (77), requires expert knowledge. Reasons for failure have to be identified by the expert and accordingly transferred to adjust the parameters. Manual selection of parameters mainly remains iterative until no more errors are recognized, e.g. (33, 37, 59, 64, 78) and is sometimes restricted to synthetic images, e.g. (79). The lack of reproducibility has often been criticized (38). Segmentation based on manual parameterization depends on the user and is only valid for a certain purpose.

Learning-from-example is an *experimental* method of setting parameters in such a way that an automatic segmentation reproduces a given (e.g. manual) segmentation (53). Propagation in volumetric images or image sequences is a major application of this method, where parameters are set once for the first slice in the stack (59, 80). Learning-from-example is possible by analysis of image values, e.g. (80) or by experimental optimization of the similarity between manual and automatic segmentation, e.g. (59, 81).

Analytical parameter selection regards a model and an image to set parameters without user interaction or a-priori knowledge on the purpose of segmentation. For the snake-model, analytic parameterization is possible using the min-max principle (38, 82). Under systematic changes of the weights of internal and external energy, each segmentation with minimal energy is determined. From the list of possible segmentations, the one with maximal energy is chosen (12). Due to combinational complexity, the min-max principle is restricted to only a few competing influences.

Gaps of Dimension

The relations between the image dimension and image influence are of major importance with respect to both image domain and value range. Note that the image domain corresponds to the relevant subset while the image value range is related to the model domain (Fig. 1).

Let us define the spatial gap of dimension (gap of domain) as the difference between the dimensions of the image domain and the relevant subset used to determine the image influences. If local zero-dimensional (0D) influences are computed for planar or volumetric images, the gap of domain equals two or three, respectively.

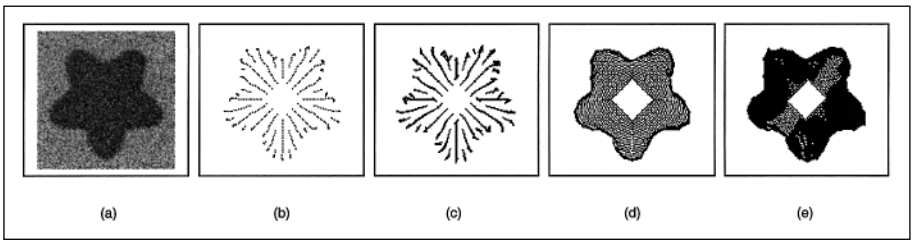

Fig. 2 Visualization of the spatial gap of dimension. A balloon model was applied to segment the synthetic object in the planar image (a). Pixels that are evaluated to form image influences are marked black for local (b), linear and perpendicular to the contour (c), linear and in direction of the contour (d), as well as planar (e) subsets

In order to simulate the effect of the gap of domain, a balloon-based model (60) was applied to segment a synthetic object of 6515 pixels in size in a 2D-image (Fig. 2). The balloon was initialized within a centered square. Image influences are globally directed and computed from planar subsets. During the iteration, point-based, line-based, and region-based subsets are simulated to compute image influences. Table 3 shows the number and percentage of pixels contributing to image influences. A gap of domain of 2, 1, and 0 results in approximately 5%, 50%, and 85% of used image information, respectively.

In analogy to the gap of domain, a gap of dimension can be defined in the value range (gap of range) as the difference between the numbers of image bands and channels in the model domain. For example, suppose three image bands that are not correlated. Then, a gap of range of 2, 1, or 0 results in 33.3%, 66.6%, or 100% of used image information, respectively.

General Recommendations

The requirements for automated localization or delineation of objects in medical images are threefold. The segmentation must cope with high variability of the shape and the appearance of medical objects, the model must yield robustness against noise and artifacts in the image, and the segmentation must always remain reliable and reproducible.

Variability of Shape and Appearance

Object representation, contour influences, and selection of parameters mainly determine the capability of an active contour model to handle the high variability of biological objects.

The model must be able to represent all possible shapes of objects. Whereas active 2D-contours usually are able to do so, the topology of objects must be adapted for representations of higher dimensions. Only a few active contours automatically perform changes in topology (28, 65). Furthermore, model dimensions of 2.5 or 3.5 should be avoided because propagation methods are restricted to small changes between adjacent slices. This holds only for tracking of objects in a sequence of planar images if the movement is small (48). Concerning volumetric data, minor inter-slice changes imply cylindrical objects, which in fact are rather seldom in biology and medicine. Additionally, the reconstruction of volumetric objects from slices is an ill-posed problem and solutions are often inaccurate. Single slices might give misleading information on the number and topology of objects (83). Nevertheless, the assumption of small changes from contours between slices is still suggested for segmentation methods, e.g. (84) or propagation sometimes regarded as the only method for segmentation of 3D-images, e.g. (18, 40, 84).

Combining optimization methods for the solution of the model with the reduction of second-order derivatives for the smoothing of the contour, active contours are unable to change automatically between convex and concave sections of the contour (54). Concave sections are only sufficiently segmented if they were already defined in the manual initialization (67). Also, fixed strengths of contour influences are rather seldomly suitable to segment biological objects. This can be solved either using adaptive weights or minimizing the third-order derivative for smoothing the contour, which, however, requires much effort to select the parameters.

In general, robustness against the variability of appearances of objects or images requires an automated image-adaptive parameterization. Furthermore, automated (i.e. experimental or analytical) training of parameters increases the applicability of active contours (81).

Noise and Artifacts

To obtain a noise-robust model, its representation should meet the image dimension and the image influences must be carefully adapted. Computing the image influences, as many image values as possible should be taken into account. Therefore, the image subset should have the same dimension as the image itself and multi-channel models should be applied for multi-band images. In other words, the gap of domain as well as the gap of range must be as small as possible. Independent interpretation of multi-band information improves the robustness of both localization (17, 85) and delineation (51, 53). Robustness is further increased by the use of spatio-temporal object representations for image domains of more than two

Table 3 Simulation of the spatial gap of dimension

relevant subset	evaluated points	percentage	gap of domain
local	376	5.8%	2
linear and normal	1122	17.2%	1
linear and tangential	3207	49.2%	1
planar	5489	84.3%	0

dimensions. Again, propagation methods should be avoided. If the object is lost due to a single noisy image within the sequence, segmentation will fail in all subsequent images even if the object clearly shows up again (86). Nevertheless, 3D-objects are mostly segmented by 2D-representations (55), and volumetric coherence is lost.

For undirected image influences, the resulting edge map or potential image needs to assign high values to positions that are likely to belong to an object's border. Usually, the presupposition of certainly located borders does not hold for biological objects. Locally directed influences are insensitive to noisy edges that do not run along the contour. The fixation of image influences to local gradients fundamentally restricts the potential of active contour segmentation (87). In general, global directionality yields a strong magnification of the model's convergence radius and, therefore, it should be applied to model image influences whenever possible.

Robustness against large-sized image artifacts mainly requires the incorporation of shape knowledge, which is not covered in this paper.

Reliability and Reproducibility

Reliable segmentation is obtained if the active contour operates without failure concerning a certain application. Failures of the model are mostly induced by the solution of the model, which is usually incapable to cover the entire high-dimensional search space. Heuristic optimization methods may get stuck in local optima. Therefore, simulation is generally superior to optimization. Self-driven approaches do not require a precise initialization. Note that for globally directed image influences, the image values themselves yield a seeking tendency for the contour that becomes independent of the current image if a valid model for the image values in- and outside the contour are found.

Reproducible segmentation means the ability of the active contour to maintain its output precision. This is mainly determined by the kind of image influences and how the parameters are selected. In general, object detection must be independent of the initialization. This property requires either the use of searching tendencies or globally directed image influences. Reproducibility also requires the experimental or analytical selection of parameters. A manual adjustment of parameters should furthermore be avoided because it presumes certain technical knowledge that is not readily available to users in the medical context.

Exemplary Use of the Scheme

To demonstrate the value of the categorization scheme, we will exemplary show its usage to successfully apply active contours for a given segmentation purpose. In vertebral disc prolaps diagnoses and for surgical planning, computed tomography is used to image a section of the spinal cord. Especially for elderly patients, the inter-vertebral discs appear like bony structures (Fig. 3).

The purpose of segmentation is the delineation of bony structures in an image domain of three dimensions with a single-banded value range. Since the root channels are usually not parallel to the CT-slices, a 3D object representation is needed to obtain a high-quality volumetric reconstruction. In addition, this choice ensures a zero gap of domain. The object has a topology containing holes and loops. Therefore, the orientation of a surface representation is important. A surface that is triangulated by a linear FEM is able to represent objects of arbitrary shape and topology. The model domain is one just like the image's value range. Hence, there is also no gap of range. Scalar Hounsfield units allow to distinguish the inside from the outside of the object even though a threshold segmentation would not yield satisfying results. The Hounsfield units are therefore used to create globally directed image influences. In order to overcome the rather high level of noise resulting from fast CT-imaging, the globally directed influences are computed for each triangular edgel regarding as much image information as possible. Therefore, volumetric (prismatic) image subsets are read around each triangle to compute a binary pressure. Smoothing of the contour is required to obtain a coherent surface of the bony structure and a regularization is necessary to obtain regular triangles. Both requirements are fulfilled using a moving average filter of vertex coordinates that implicitly reduces the contour's second-order derivative. Furthermore, a topology adaptation is needed whenever edgels intersect so that loops and channels can be automatically reconstructed. Being initialized as a box surrounding the entire data volume, some edgels have to pass great distances in image space to reach the bony structures in the image of varying location and size. Only a simulation of directed forces is able to fulfill this requirement. The binary pressure results in an image-driven segmentation. Since CT-scanners provide normalized image values, the strength of smoothing as well as the size of edgels does not vary for different images. Therefore, an application-adaptive parameter optimization is appropriate for the given purpose. Parameters for image influences can be analytically set to form a binary pressure for Hounsfield units of bony and watery structures, respectively. The strength of smoothing can be computed from one central slice and one exemplary manual segmentation and is therefore experimentally set.

The resulting active contour for segmentation of bony structures of the spinal cord is one example for the applicability of the general model suggested in (28). Figure 3

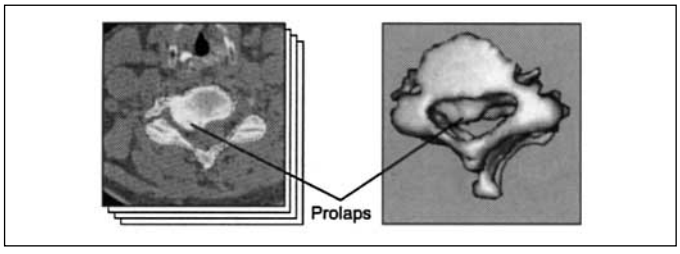

Fig. 3
Active contour segmentation of bony structures in a CT volume of the vertebra (contrast enhanced) and volume rendering of the determined 3D segment

shows its segmentation for the given purpose.

Discussion

The selection and subsequent implementation of a model for segmentation is performed in dialogue between a physician and a technician, e.g. a computer scientist. The presented classification scheme enables such development partners to cooperatively create a requirements specification for a model-based segmentation method: For each of the categories, a class has to be selected to provide a complete interface between clinical application and implementation. The authors are well aware that this requires both development partners to take part in an interdisciplinary process and the classification scheme has already proven useful for this dialogue.

It is important to note that the categories and instances, which have been introduced in this paper, in general are unambiguous. However, some object representations with many degrees of freedom exist that do not match the categories given above. Examples are active bubbles (88). Also, some relations and transitions exist, for example:

- Manual parameterization is not feasible if the parameters are set iteration-adaptively.
- The categorization according to the directionality of image influences is independent of the method for the solution that either uses scalar quality measures or directed influences in a simulation. Consequently, it is possible to calculate directed forces using scalar image influences by finding the point with the highest potential in the vicinity of vertices. Then, a directed force can point towards this position. Vice versa, the scalar product of the contour's normal vector and the image's gradient is locally directed but only yields a scalar quality measure for the position of vertices.
- The method of regularization often depends on the object's definition itself. For instance, if spline-interpolated vertices are used to represent an object, smoothing is redundant.
- Since the search for an energy minimum is related to an equality of forces, transitions exist between optimization and simulation techniques. Optimization becomes simulation when the contour's energy is regarded as a potential and a force is defined pointing against the gradient of this potential. This results in an equality of forces in local minima of the energy function (54). Usually, this property is used in heuristic optimization schemes, where vertices perform a steepest descent in the contour's potential. Vice versa, the sum of all forces of a mechanically simulated contour can be written as the contour's energy (89) when the direction of forces is disregarded. Seeking tendencies no longer take effect because their absolute value is constant. This results in a reduction of the method's convergence radius.

Although a general concordance is found in the literature that FEM-contours are superior to FDM-contours, linear vs. non-linear FEMs are often contrarily rated. Non-linear FEMs are usually applied to ensure smooth contours of the segmented objects. However, the advantage of $C^{(1)}$-continuity is questionable in the context of digital image processing, which is based on discrete grids. The adjustable size of all finite elements allows to give linear approximations of any desired precision. Even linear finite elements of a size below pixel or voxel dimension are used, e.g. (27, 65).

Conclusion

The well known snake model introduced in 1987 was designed for the delineation of objects following manual localization in the graphical user interface called "snake pit". The model is applied to planar single-band images. The model dimension was two and objects were represented by vertices that were FDM-connected (snaxels). The point-based image influences were not directed (external energy). The external energy was defined as the sum of all scalar image gradients read at the vertex positions. The contour influence (internal energy) was defined as the weighted sum of the first- and second-order derivative of the contour. Solutions of the model were found using a local optimization scheme that minimizes the sum of internal and external energies. By use of the snake pit, parameters were manually set and adapted for every image.

The requirements in medical image processing led to improvements in almost every category as compared to the widely used snake model. However, these improvements may result in remarkable effort for modeling and implementation (25, 45). The stepwise key-code presented in this paper (Fig. 1) may help to determine the optimal active contour variant for a certain application. To exemplify an active contour that fulfills these requirements, we refer to (28). The learning-from-example parameter selection of this model is described in (53) and the extension to image-adaptive parameter selection is given in (75).

Acknowledgment
The authors would like to thank Cord Spreckelsen for his helpful comments on the first manuscript of this paper.

References

1. Undrill PE, Delibasis K, Cameron GG. An application of genetic algorithms to geometric model-guided interpretation of brain anatomy. Pattern Recognition 1997; 30(2): 217–27.
2. Kass M, Witkin A, Terzopoulos D. Snakes: active contour models. Int J Comput Vision 1978; 1(4): 321–31.
3. Liang J, McInerney T, Terzopoulos D. Interactive medical image segmentation with united snakes. Lecture Notes Comput Science 1999; 1679: 116–27.
4. Gunn SR, Nixon MS. Improving snake performance via a dual active contour. Lecture Notes Comput Science 1995; 970: 600–5.
5. Yang GZ, Burger P, Panting J, Gatehouse PD, Rueckert D, Pennell DJ, Firmin DN. Motion and deformation tracking for short-axis echo-planar myocardial perfusion imaging. Med Image Analysis 1998; 2(3): 285–302.
6. Chalana V, Hodgdon JA, Haynor DR. Unified data structures in a software environment for medical image segmentation. Proceedings SPIE 1998; 3338: 947–58.
7. Sebbahi A, Herment A, De Cesare A, Mousseaux E. Multimodality cardiovascular image segmentation using a deformable contour model. Comput Med Imaging Graphics 1997; 21(2): 79–89.
8. Kang DJ. A fast and stable snake algorithm for medical images. Pattern Recognition Letters 1999; 20(5): 507–12.

9. McInerney T, Terzopoulos D. Deformable models in medical image analysis: a survey. Med Image Analysis 1996; 1(2): 91–108.
10. Jain AK, Zhong Y, Dubuisson-Jolly MP. Deformable template models: a review. Signal Processing 1998; 71(2): 109–29.
11. Xu C, Pham DL, Prince JL. Image Segmentation using deformable models. In: Sonka M, Fitzpatrick JM, editors. Handbook of Medical Imaging, Part 2: Medical Image Processing and Analysis. Bellingham: SPIE Press; 2000.
12. Lai KF, Chin RT. Deformable contours: modeling and extraction. IEEE Transactions on Pattern Analysis and Machine Intelligence 1995; 17(11): 1084–90.
13. Cootes TF, Taylor CJ, Cooper DH, Graham J. Active shape models: their training and application. Comput Vision Image Understanding 1995; 61(1): 38–59.
14. Staib LH, Duncan JS. Boundary finding with parametrically deformable models. IEEE Transactions on Pattern Analysis Machine Intelligence 1992; 14(11): 1061–75.
15. Vemuri BC, Guo Y. Snake pedals: compact and versatile geometric models with physics-based control. IEEE Transactions Pattern Analysis Machine Intelligence 2000; 22(5): 445–59.
16. Cinque L, Romangnoli R, Levialdi S, Nguyen PTA, Guan L. Self-organizing map for segmenting 3D biological images. Proceedings Int Conference Pattern Recognition ICPR'98 (vol 1). 1998: 471–3.
17. Agbinya JI, Rees D. Multi-object tracking in video. Real-Time Imaging 1999; 5(5): 295–304.
18. Daesik J, Hyung-Il C. Moving object tracking by optimizing active models. Proceedings Int Conference Pattern Recognition ICPR'98 (vol 1). 1998: 738–40.
19. Falcão AX, Udupa JK, Samarasekera S, Sharma S, Hirsch BE, de Lotufo RA. User-steered image segmentation paradigms: live wire and live lane. Graphical Models Image Processing 1998; 60(4): 233–60.
20. Lynch JA, Zaim S, Zhao J, Stork A, Peterfy CG, Genant HK. Cartilage segmentation of 3D MRI scans of the osteoarthritic knee combining user knowledge and active contours. Proceedings SPIE 2000; 3979: 925–35.
21. Malassiotis S, Strintzis MG. Tracking the left ventricle in echocardiographic images by learning heart dynamics. IEEE Transactions Med Imaging 1999; 18(3): 282–90.
22. Duncan JS, Ayache N. Medical image analysis: Progress over two decades and the challenges ahead. IEEE Transactions Pattern Analysis Machine Intelligence 2000; 22(1): 85–106.
23. Blake A, Isard M, Reynard D. Learning to track the visual motion of contours. Artificial Intelligence 1995; 78(1–2): 179–212.
24. Peterfreund N. The velocity snake: deformable contour for tracking in spatio-velocity space. Comput Vision Image Understanding 1999; 73(3): 346–56.
25. Cohen LD, Cohen I. Finite-element methods for active contour models and balloons for 2-D and 3-D images. IEEE Transactions Pattern Analysis Machine Intelligence 1993; 15(11): 1131–47.
26. Huang J, Abendschein D, Davila-Roman VG, Amini AA. Spatio-temporal tracking of myocardial deformations with a 4-D B-spline model from tagged MRI. IEEE Transactions Med Imaging 1999; 18(10): 957–72.
27. Yudong Z, Pelc NJ. A spatiotemporal model of cyclic kinematics and its application to analyzing nonrigid motion with MR velocity images. IEEE Transactions Med Imaging 1999; 18(7): 557–69.
28. Bredno J, Lehmann TM, Spitzer K. General finite element model for segmentation in 2, 3, and 4 dimensions. Proceedings SPIE 2000; 3979: 1174–84.
29. Geiger D, Gupta A, Costa LA, Vlontzos J. Dynamic programming for detecting, tracking, and matching deformable contours. IEEE Transactions Pattern Analysis Machine Intelligence 1995; 17(3): 294–302.
30. Ranganath S. Contour extraction from cardiac MRI studies using snakes. IEEE Transactions Med Imaging 1995; 14(2): 328–38.
31. Leymarie F, Levine MD. Tracking deformable objects in the plane using an active contour model. IEEE Transactions Pattern Analysis Machine Intelligence 1993; 15(6): 617–34.
32. Denzler J, Niemann H. Active-rays: Polar-transformed active contours for real-time contour tracking. Real-Time Imaging 1999; 5(3): 203–13.
33. Kucera D, Martin RW. Segmentation of sequences of echocardiographic images using a simplified 3D active contour model with region-based external forces. Comput Med Imaging Graphics 1997; 21(1): 1–21.
34. Kauffmann C, Godbout B, de Guise JA. Simplified active contour model applied to bone structure segmentation in digital radiographs. Proceedings SPIE 1998; 3338: 663–72.
35. Bulpitt AJ, Berry E. Spiral CT of abdominal aortic aneurysms: comparison of segmentation with an automatic 3D deformable model and interactive segmentation. Proceedings SPIE 1998; 3338: 938–46.
36. Vilariño DL, Brea VM, Cabello D, Pardo JM. Discrete-time CNN for image segmentation by active contours. Pattern Recognition Letters 1998; 19(8): 721–34.
37. Lam CL, Yuen SY. An unbiased active contour algorithm for object tracking. Pattern Recognition Letters 1998; 19(5–6): 491–8.
38. Akgul YS, Kambhamettu C, Stone M. Automatic extraction and tracking of the tongue contours. IEEE Transactions Med Imaging 1999; 18(10): 1035–45.
39. Pentland A, Horowitz B. Recovery of nonrigid motion and structure. IEEE Transactions Pattern Analysis Machine Intelligence 1991; 13(7): 730–42.
40. Shekhar R, Cothren RM, Vince DG, Chandra S, Thomas JD, Cornhill JF. Three-dimensional segmentation of luminal and adventitial borders in serial intravascular ultrasound images. Comput Med Imaging Graphics 1999; 23(6), 299–309.
41. Ghanei A, Soltanian-Zadeh H, Windham JP. Segmentation of the hippocampus from brain MRI using deformable contours. Comput Med Imaging Graphics 1998; 22(3): 203–16.
42. Kobbelt LP. Discrete fairing and variational subdivision for freeform surface design. Visual Comput 2000; 16(3–4): 142–58.
43. Juarez EL, Dumont C, Abidi MA. Object modeling in multiple-object 3D scenes using deformable simplex meshes. Proceedings SPIE 2000; 3958: 144–52.
44. Rueckert D, Burger P, Forbat SM, Mohiaddin RD, Yang GZ. Automatic tracking of the aorta in cardiovascular MR images using deformable models. IEEE Transactions Med Imaging 1997; 16(5): 581–90.
45. McInerney T, Terzopoulos D. A dynamic finite element surface model for segmentation and tracking in multidimensional medical images with application to cardiac 4D image analysis. Comput Med Imaging Graphics 1995; 19(1): 69–83.
46. Malladi R, Sethian JA, Vemuri BC. Shape modeling with front propagation: a level set approach. IEEE Transactions Pattern Analysis Machine Intelligence 1995; 17(2): 158–75.
47. Grzeszczuk RP, Levin DN. Brownian strings: Segmenting images with stochastically deformable contours. IEEE Transactions Pattern Analysis Machine Intelligence 1997; 19(10): 1100–14.
48. Zhong Y, Jain AK, Dubuisson-Jolly MP. Object tracking using deformable templates. IEEE Transactions Pattern Analysis Machine Intelligence 2000; 22(5): 544–9.
49. Ngoi KP, Jia JC. An active contour model for colour region extraction in natural scenes. Image Vision Comput 1999; 17(13): 955–66.
50. Bowden R, Mitchell TA, Sarhadi M. Non-linear statistical models for the 3D reconstruction of human pose and motion from monocular image sequences. Image Vision Comput 2000; 18(9): 729–37.
51. Ivins J, Porrill J. Constrained active region models for fast tracking in color image sequences. Comput Vision Image Understanding 1998; 72(1): 54–71.
52. Zhu SC, Lee TS, Yuille AL. Region competition: unifying snakes, region growing, energy/Bayes/MDL for multi-band image segmentation. IEEE Transactions Pattern Analysis Machine Intelligence 1996; 18: 884–900.
53. Bredno J, Lehmann TM, Spitzer K. Automatic parameter setting for balloon models. Proceedings SPIE 2000; 3979: 1185–94.
54. Xu C, Prince JL. Snakes, shapes, and gradient vector flow. IEEE Transactions Image Processing 1998; 7(3): 359–69.
55. Pardo JM, Cabello D, Heras J. A snake for model-based segmentation of biomedical images. Pattern Recognition Letters 1997; 18(14): 1529–38.
56. Ronfard R. Region-based strategies for active contour models. Int J Comput Vision 1994; 13(2): 229–51.
57. Horritt MS. A statistical active contour model for SAR image segmentation. Image Vision Comput 1999; 17(3–4): 213–24.
58. Boyer KL, Sarkar S. Perceptual organization in computer vision: status, challenges and potential. Comput Vision Image Understanding 1999; 76(1): 1–5.

59. Cagnoni S, Dobrzeniecki AB, Poli R, Yanch JC. Genetic algorithm-based interactive segmentation of 3D medical images. Image Vision Computing 1999; 17(12): 881–95.
60. Metzler V, Bredno J, Lehmann TM, Spitzer K. A deformable membrane for the segmentation of cytological samples. Proceedings SPIE 1998; 3338: 1246–57.
61. von Klinski S, Derz C, Weese D, Tolxdorff T. Model-based image processing using snakes and mutual information. Proceedings SPIE 2000; 3979: 1053–64.
62. Schreckenberg M, von Dziembowski G, Ziermann O, Meyer-Ebrecht D. Automatische Objekterkennung in 3D-Echokardiographiesequenzen auf der Basis aktiver Oberflächenmodelle und modellgekoppelter Merkmalsextraktion. In: Lehmann TM et al., eds. Bildverarbeitung für die Medizin 1998. Berlin: Springer; 1997: 328–32. (in German)
63. Terzopoulos D. Regularization of inverse visual problems involving discontinuities. IEEE Transactions Pattern Analysis Machine Intelligence 1986; 8(4): 413–24.
64. Lürig C, Kobbelt L, Ertl T. Hierarchical solutions for the deformable surface problem in visualization. Graphical Models 2000; 62(1): 2–18.
65. McInerney T, Terzopoulos D. Topology adaptive deformable surfaces for medical image volume segmentation. IEEE Transactions Medical Imaging 1999; 18(10): 840–50.
66. Lobregt S, Viergever MA. A discrete dynamic contour model. IEEE Transactions Medical Imaging 1995; 14(1): 12–24.
67. Davatzikos C, Prince JL. Convexity analysis of active contour problems. Image Vision Comput 1999; 17(1): 27–36.
68. Williams DJ, Shah M. A fast algorithm for active contours and curvature estimation. CVGIP-Image Understanding 1992; 55(1): 14–26.
69. Wang J, Li X. A system for segmenting ultrasound images. Proceedings International Conference Pattern Recognition ICPR'98. 1998: 456–61.
70. Neuenschwander W, Fua P, Székely G, Kübler O. Velcro surfaces: fast initialization of deformable models. Comput Vision Image Understanding 1997; 65(2): 237–45.
71. Kelemen A, Székely G, Gerig G. Elastic model-based segmentation of 3-D neuroradiological data sets. IEEE Transactions Med Imaging 1999; 18(10): 828–39.
72. Coppini G, Poli R, Valli G. Recovery of the 3-D shape of the left ventricle from echocardiographic images. IEEE Transactions Med Imaging 1995; 14(2): 301–17.
73. Giachetti A. On-line analysis of echocardiographic image sequences. Med Image Analysis 1998; 2(3): 162–284.
74. Nastar C, Ayache N. Non-rigid motion analysis in medical images: a physically based approach. Lecture Notes Comput Science 1993; 687: 17–32.
75. Lehmann TM, Bredno J, Spitzer K. Texture-adaptive active contour models. Lecture Notes Computer Science 2001; 2013: 387–96.
76. Garrido A, De La Blanca NP. Physically-based active shape models: initialization and optimization. Pattern Recognition 1998; 31(8): 1003–17.
77. Gang X, Segawa E, Tsuji S. Robust active contours with insensitive parameters. Pattern Recognition 1994; 27(7): 879–84.
78. Loncaric S, Kovacevic D, Sorantin E. Semi-automatic active contour approach to segmentation of computed tomography values. Proceedings SPIE 2000; 3979: 917–24.
79. Xu X, Pham DL, Rettmann ME, Yu DN, Prince JL. Reconstruction of the human cerebral cortex from magnetic resonance images. IEEE Transactions Med Imaging 1999; 18(6): 467–80.
80. Levienaise-Obadia B, Gee A. Adaptive segmentation of ultrasound images. Image Vision Comput 1999; 17(8): 583–8.
81. Chen DH, Sun YN. A self-learning contour finding algorithm for echocardiac analysis. Proceedings SPIE 1998; 3338: 971–81.
82. Gennert MA, Yuille AL. Determining the optimal weights in multiple objective function optimization. Proceedings 2nd International Conference Comput Vision. 1988: 87–9.
83. Barequet G, Shapiro D, Tal A. Multilevel sensitive reconstruction of polyhedral surfaces from parallel slices. Visual Comput 2000; 16(2): 116–33.
84. Chalana V, Sannella M, Haynor DR. General-purpose software tool for serial segmentation of stacked images. Proceedings SPIE 2000; 3979: 192–203.
85. Heigl B, Paulus D, Niemann H. Tracking points in sequences of color images. Pattern Recognition Image Analysis 1999; 9(4): 648–53.
86. Chan S, Ngo CW, Lai KF. Motion tracking of human mouth by generalized deformable models. Pattern Recognition Letters 1999; 20(9): 879–87.
87. Chakraborty A, Staib LH, Duncan JS. An integrated approach for surface finding in medical images. Proceedings IEEE Workshop Mathematical Methods in Biomedical Image Analysis 1996. 1996: 253–62.
88. Tek H, Kimia BB. Volumetric segmentation of medical images by three-dimensional bubbles. Comput Vision Image Understanding 1997; 65(2): 246–58.
89. Bulpitt AJ, Efford ND. An efficient 3D deformable model with a self-optimising mesh. Image Vision Comput 1996; 14(8): 573–80.

Correspondence to:
Dr. Thomas M. Lehmann
RWTH Aachen
Institut für Medizinische Informatik
D-52027 Aachen, Germany
E-Mail: lehmann@computer.org